Disruption of Dcp1 leads to a Dcp2-dependent aberrant ribosome profiles in Aspergillus nidulans

Bharudin, I., Caddick, M. X., Connell, S. R., Lamaudière, M. T. F. & Morozov, I. Y

DOI 10.1111/mmi.15059
ISSN 0950-382X
ESSN 1365-2958

Publisher: Wiley

Received: 27 October 2022 | Revised: 24 March 2023 | Accepted: 26 March 2023

DOI: 10.1111/mmi.15059

RESEARCH ARTICLE

WILEY

Disruption of Dcp1 leads to a Dcp2-dependent aberrant ribosome profiles in *Aspergillus nidulans*

Izwan Bharudin[1,2] | Mark X. Caddick[1] | Sean R. Connell[3,4] | Matthew T. F. Lamaudière[5] | Igor Y. Morozov[5]

[1]Institute of Systems, Molecular and Integrative Biology, The University of Liverpool, Biosciences Building, Crown Street, Liverpool, L69 7ZB, UK

[2]Department of Biological Sciences and Biotechnology, Faculty of Science and Technology, Universiti Kebangsaan Malaysia, Bangi, 43600 UKM, Selangor, Malaysia

[3]BioCruces Bizkaia Health Research Institute, Plaza Cruces s/n, Barakaldo, 48903, Spain

[4]IKERBASQUE, Basque Foundation for Science, Bilbao, 48011, Spain

[5]Coventry University, Centre for Health & Life Sciences, Alison Gingell Building, 20 Whitefriars Street, Coventry, CV1 5FB, UK

Correspondence
Igor Y. Morozov, Coventry University, Centre for Health & Life Sciences, Alison Gingell Building, 20 Whitefriars Street, Coventry, CV1 5FB, UK.
Email: ab6069@coventry.ac.uk

Funding information
BBSRC, Grant/Award Number: BB/H020365; Ministerio de Economía y Competitividad, Grant/Award Number: CTQ201782222-R and PID2021-122705OB-I00

Abstract

There are multiple RNA degradation mechanisms in eukaryotes, key among these is mRNA decapping, which requires the Dcp1-Dcp2 complex. Decapping is involved in various processes including nonsense-mediated decay (NMD), a process by which aberrant transcripts with a premature termination codon are targeted for translational repression and rapid decay. NMD is ubiquitous throughout eukaryotes and the key factors involved are highly conserved, although many differences have evolved. We investigated the role of *Aspergillus nidulans* decapping factors in NMD and found that they are not required, unlike *Saccharomyces cerevisiae*. Intriguingly, we also observed that the disruption of one of the decapping factors, Dcp1, leads to an aberrant ribosome profile. Importantly this was not shared by mutations disrupting Dcp2, the catalytic component of the decapping complex. The aberrant profile is associated with the accumulation of a high proportion of 25S rRNA degradation intermediates. We identified the location of three rRNA cleavage sites and show that a mutation targeted to disrupt the catalytic domain of Dcp2 partially suppresses the aberrant profile of Δ*dcp1* strains. This suggests that in the absence of Dcp1, cleaved ribosomal components accumulate and Dcp2 may be directly involved in mediating these cleavage events. We discuss the implications of this.

KEYWORDS
Aspergillus nidulans, Dcp1, decapping, nonsense-dediated decay, polysomal fractionation

1 | INTRODUCTION

The degradation of RNA is critical to all organisms, with key roles in the fundamental processes including transcript formation, gene regulation and translation. Although there are many differences between eukaryotes, the key RNA degradation mechanisms and components have generally been conserved. One major pathway for mRNA degradation is initiated by decapping, through which the 5′ cap structure is cleaved, exposing a 5′ monophosphate (Coller & Parker, 2004). This both silences the mRNA by preventing further initiation of translation and triggers rapid 5′ to 3′ degradation. Consequently, decapping is integral to different RNA degradation processes, including deadenylation-dependent decapping, in which the shortened Poly(A) tail triggers decapping through a mechanism involving various factors which both monitor Poly(A) tail length and link it physically with the 5′ CAP structure (Nissan et al., 2010). Decapping of mRNA is mediated by Dcp2 which, with Dcp1, forms the conserved core of the decapping complex (Vidya &

Duchaine, 2022), where Dcp1 is a regulatory component required for Dcp2 activation. The decapping activity is associated with the actively translating polysomes, where mRNA decapping is initiated (Hu et al., 2009). Both Dcp1 and Dcp2 are also associated with processing bodies (P-bodies), with Dcp2 being the most abundant constituent. These are active, dynamic foci of mRNA degradation within the cell (Xing et al., 2020).

Nonsense-mediated decay (NMD) occurs when a transcript is recognised by a translation-dependent mechanism as having a premature termination codon (PTC) (Kervestin & Jacobson, 2012). These aberrant transcripts may result from a gene mutation, errors occurring during transcription or splicing as well as ribosomal frame-shifts on wild-type (WT) transcripts (Celik et al., 2017). In *Saccharomyces cerevisiae*, the Dcp1/Dcp2 decapping complex is a key component of NMD (Cao & Parker, 2003; Muhlrad & Parker, 1999). Decapping facilitates rapid degradation of the aberrant mRNA via 5′-3′ exonuclease degradation, mediated by Xrn1 (Nagarajan et al., 2013). However, in animal systems, NMD can bypass the dependence on decapping due to additional RNA cleavage mechanisms, most notably by SMG6-mediated cleavage of the RNA upstream of the stop codon (Huntzinger et al., 2008). Orthologues of SMG6 have not been identified in fungal systems, which explain the dependence of NMD on decapping in *S. cerevisiae*.

Aspergillus nidulans is a well-studied filamentous fungus. With respect to RNA degradation, a number of key mechanisms have been investigated including NMD and decapping (Morozov et al., 2006, 2012; Morozov, Jones, Spiller, et al., 2010). Based on these studies it is apparent that this fungus is in many respects more similar to animal and plant systems, most notably with respect to mRNA 3′ pyrimidine tagging, which appears to be absent in *S. cerevisiae* (Morozov, Jones, Razak, et al., 2010; Rissland & Norbury, 2009). We, therefore, undertook to determine if decapping was required for NMD in *A. nidulans* by screening mutant strains disrupted for specific components involved in mRNA decapping. This proved that NMD was retained in decapping defective strains suggesting the presence of as yet unidentified RNA degradation mechanisms in this ascomycete. Intriguingly, sucrose gradient ribosomal profiles obtained during the study revealed an aberrant profile specifically in Δ*dcp1* strains. We investigated this and determined that in Δ*dcp1* strains, cleaved ribosome subunits accumulate to form the aberrant profile and that this is partially dependent on Dcp2 catalytic activity.

2 | RESULTS

2.1 | Decapping factors and Xrn1 are not required for nonsense-mediated decay

In *S. cerevisiae* NMD is dependent on the decapping factor Dcp2p and the cytoplasmic 5′-3′ exonuclease Xrn1p (Muhlrad & Parker, 1994). To determine if a similar situation pertains to *A. nidulans* mutant strains disrupted for *xrn1*, *dcp2* we conducted quantitative northern analysis, comparing the relative abundance of uaZ^+ and uaZ14 in five different genetic backgrounds: WT, Δ*xrn1*, Δ*dcp2* and two mutant backgrounds are known to disrupt NMD; Δ*upf1* and *nmdA1*. Previously we have demonstrated that the *uaZ14* transcript is subject to NMD (Morozov et al., 2012). From the data presented in Figure 1, it is clear that NMD persists in strains deleted for either *xrn1* or *dcp2*, unlike strains disrupted for the two known NMD factors. However, the response in the Δ*xrn1* strain is significantly less pronounced, suggesting Xrn1 contributes to but is not essential for NMD in *A. nidulans*. To extend this analysis we undertook qRT-PCR-based analysis to monitor the relative abundance *uaZ14* (Figure 2) and a second transcript subject to NMD, *hxA5* (Figure S1), (Morozov et al., 2012). Furthermore, in addition to xrn1 and dcp2, we investigated four other genes implicated in the decapping pathway; *dcp1*, *pat1*, *lsm1* and *dhh1* (Mossanen-Parsi et al., 2021) (Figure 2). These data revealed that NMD is largely unaffected by disruption of any one of these six genes. The persistence of NMD in mutants that are disrupted for the decapping factor Dcp2 and the exonuclease Xrn1 was surprising based on observations in *S. cerevisiae* and may suggest alternative de-capping and/or RNA degradation mechanisms are involved in *A. nidulans*.

In *S. cerevisiae*, there is a second 5′ exonuclease, Rat1p, which is primarily localised to the nucleus (Amberg et al., 1992). *A. nidulans* has an orthologue of Rat1, AN0707. It is, therefore, possible

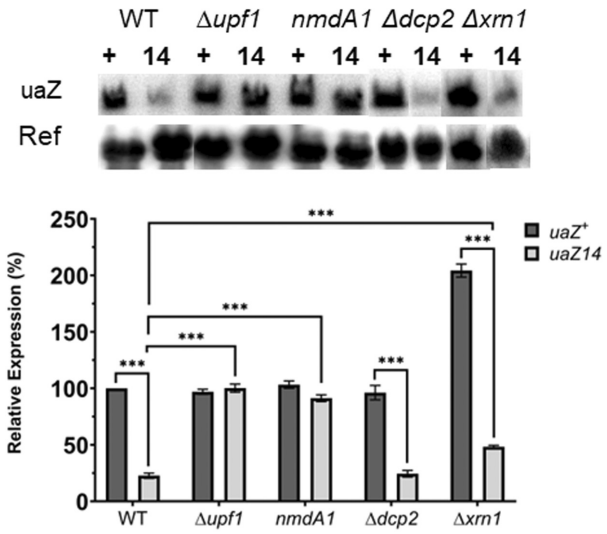

FIGURE 1 Nothern analysis to determine the effect of Δ*xrn1* and Δ*dcp2* mutations on nonsense-mediated decay (NMD). uaZ^+ and uaZ^{14} transcript levels were monitored using northern analysis (A) and the quantitated data used to compare the NMD response of wild type (WT) with Δ*xrn1*, Δ*dcp2*, Δupf1 and nmdA1 strains. 18S rRNA was used as a loading control. Results are representative of three independent experiments with the standard error (error bar). Two-tailed *t*-test, assuming unequal variance, were conducted for the comparisons of uaZ^+ and *uaZ14* in each genetic background and uaZ14 levels between WT and mutant backgrounds ($^*p \le 0.05$, $^{**}p \le 0.01$ and $^{***}p \le 0.001$). Only in Δ*upf1* and *nmdA1* strains was NMD fully disrupted, with no significant difference in the levels of *uaZ14* and uaZ^+ mRNA. However, although xrn1 strain retained an NMD response, this was significantly less pronounced than that of WT.

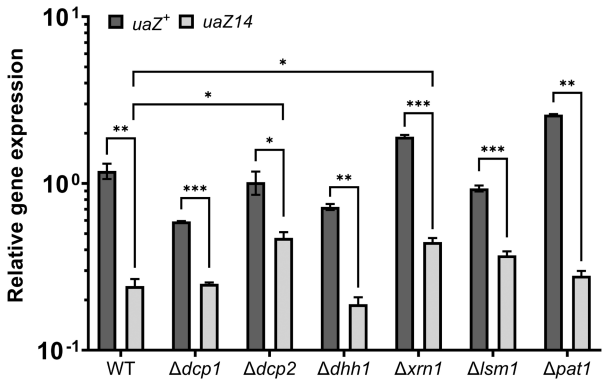

FIGURE 2 Characterisation of nonsense-mediated decay (NMD) in different mutant backgrounds. qRT-PCR of total RNA samples was conducted to monitor the level of *uaZ*$^{+}$ (+) and *uaZ14* (14) transcripts in different genetic backgrounds: Wild type (WT), Δ*dcp1*, Δ*dcp2*, Δ*dhh1*, Δ*xrn1*, Δ*lsm1* and Δ*pat1*. 18S rRNA was used as the endogenous control to normalise the expression of *uaZ* transcripts. Results are representative of three independent experiments with the standard error (error bar). Two-tailed *t*-test, assuming unequal variance, was conducted for the comparisons of *uaZ*$^{+}$ and *uaZ14* in each background and *uaZ14* levels between WT and each mutant background. In all genetic backgrounds tested the level of *uaZ14* mRNA was significantly lower than *uaZ*$^{+}$ (*$p \le 0.05$, **$p \le 0.01$ and ***$p \le 0.001$), indicative of NMD being retained in all mutant strains.

that disruption of *xrn1* was not sufficient to suppress NMD due to the presence of this second 5′ exonuclease activity. We disrupted AN0707 but the mutant phenotype was extremely severe, with very poor growth. Consequently, we were unable to pursue this further. It is worth noting that the *S. cerevisiae RAT1* is essential (Amberg et al., 1992).

2.2 | Aberrant ribosomal polysome profiles were observed for Δ*dcp1* and Δ*dcp2* strains

It has been demonstrated in *S. cerevisiae* that transcripts subject to NMD are decapped while associated with the polysomes and the resulting 5′-3′ degradation of substrates proceeds while the transcripts remain bound to the ribosomes (Hu et al., 2009). With the intention of investigating whether this is the case in *A. nidulans*, we undertook sucrose density gradient analysis to examine transcript distribution across the ribosome profile. The polysome profiles obtained revealed that the strains disrupted for *dcp1* or *dcp2* were distinct from WT (Figure 3). The most striking difference was seen for the *Δdcp1* strain, which produced a predominant peak migrating in the region of the 60S ribosomal subunit, compared with WT where the predominant peak was the 80S ribosomal fraction (Figure 3c). Disruption of *dcp2* (Figure 3d) led to an increase in

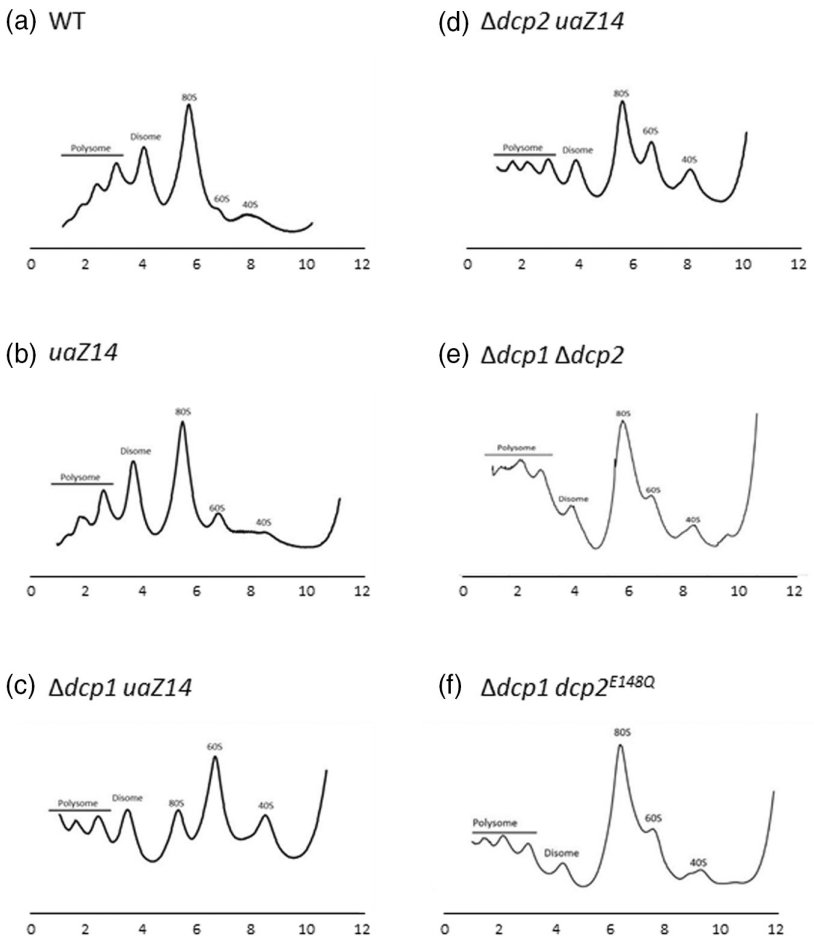

FIGURE 3 Polysome profiles from different *Aspergillus nidulans* strain. Cell-free extracts derived from five strains (a) wild type, (b) *uaZ14*, (c) Δ*dcp1 uaZ14*, (d) Δ*dcp2 uaZ14*, (e) Δ*dcp1* Δ*dcp2*, (f) Δ*dcp1 dcp2*^{E148Q} were subject to ribosome profiling using sucrose density centrifugation. Cell lysates were separated on a 10–50% sucrose gradient and the absorbance at A_{254} along the gradient was monitored. The sedimentation position of ribosomal complexes (40S, 60S, 80S, disome (2×80S) and polysomes) are indicated on each panel. Results are representative of multiple ($n \ge 3$) independent experiments.

the absorbance of both the 60S and 40S ribosomal subunit fractions. However, the increase in both fractions was proportionate, with the 80S ribosomal fraction remained predominant. The very different profiles observed for the *Δdcp1* and *Δdcp2* strains are surprising as the respective proteins are known to act together in mRNA decapping (Chang et al., 2014; Valkov et al., 2016). To confirm that this difference is associated with disruption of *dcp1* and does not relate to an unidentified background allele several additional Δ*dcp1* mutant strains, obtained by outcrossing the original Δ*dcp1* strain, were also subjected to polysome profiling. In all cases, a similar aberrant polysome profile was observed (Figure S2) consistent with the higher 60S peak being a consequence of *dcp1* deletion. EDTA treatment of the WT and Δ*dcp1* polysomes disrupted the polysomal fractions (data not shown), consistent with the observed polysomes being translationally active structures (Morozov et al., 2012).

To investigate this further, purified mRNA from the polysome profiling was subjected to agarose gel electrophoresis under non-denaturing conditions. The resulting gel revealed a distinct difference in the "60S fractions" between the WT and *Δdcp1* mutant strains; in the Δ*dcp1* strain, an intense band appeared which migrated marginally slower than 18S rRNA (Figure 4). In the WT, a week band is present in a similar position but its relative intensity is less than 10% of the equivalent band in the mutant strain. The same aberrant profile was also found in the two additional *Δdcp1* strains tested (data not shown). We, therefore, postulated that this band represents a ribosomal RNA degradation product that accumulated as a consequence of the disruption of *dcp1*. One possibility is that it is a degradation product derived from the 25S rRNA.

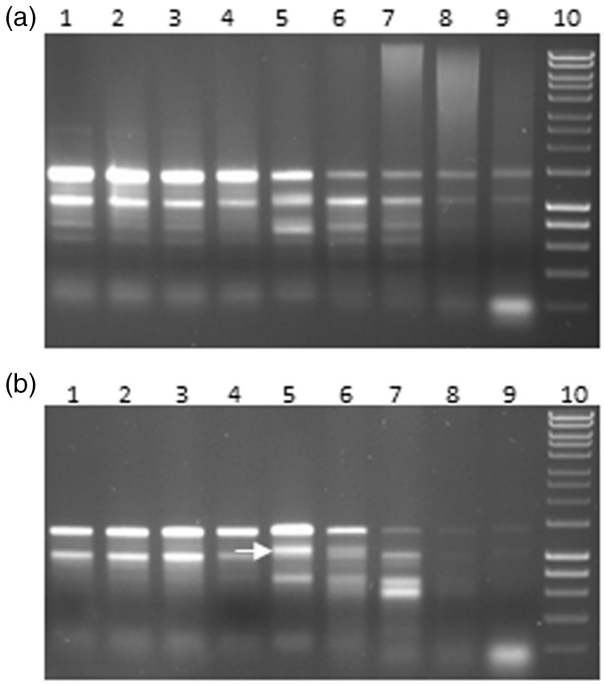

FIGURE 4 Purified RNA from the polysome fractionation of wild type (WT) and Δ*dcp1* strains. (a) Representative Agarose gel of purified RNA from the sucrose gradient fractions obtained using the WT strain. 18S and 25S rRNA bands are apparent in the polysome and monosome fractions (Lanes 1–5). DNA Ladder (Hyperladder1) is shown in lane 10. (b) The equivalent analysis of purified rRNA from the *Δdcp1* strain. 18S and 25S rRNA bands are clearly visible in the polysome and monosome fractions. However, there is an additional major band immediately above the 18S rRNA band in the 60S fraction (arrow) in lanes 5 & 6.

Dcp1 and Dcp2 are known to work together in the decapping complex with Dcp2 being the catalytic component (Coller & Parker, 2004; Valkov et al., 2016). To determine whether the aberrant ribosomal profile produced by *Δdcp1* strains is *dcp2*-dependent, a *Δdcp1* strain was crossed with *Δdcp2* strain, producing the double mutant. The polysome profiles of the double mutant, *Δdcp1 Δdcp2*, had a relatively small 60S peak (Figure 3e) equivalent to that of the *Δdcp2* stain, distinguishing it from the *Δdcp1* single mutant (Figure 3c). This would be consistent with Dcp2 activity being required for the production of the aberrant profile in the Δ*dcp1* background.

Cleavage of the mRNA 5′ cap is dependent on the Nudix domain of Dcp2 (Song et al., 2013). We, therefore, undertook to test if this functional catalytic domain is required for the aberrant ribosomal profile observed for *Δdcp1* strains, the hypothesis being that in the absence of Dcp1, Dcp2 acquires a new or enhanced activity not previously observed. A single amino acid substitution was introduced into Dcp2, disrupting the catalytic site of the Nudix domain (Figure S3). The mutation results in the glutamic acid at position 148 being replaced by a glutamine. The equivalent mutation is known to disrupt the decapping activity of *S. cerevisiae* Dcp2 (Song et al., 2013). The $dcp2^{E148Q}$ mutant allele was "knocked in" to the original Δ*dcp2* strain. The resulting mutant strain was morphologically very similar to Δ*dcp2* and Δ*dcp1* strains consistent with full loss of activity (Figure 5).

To assess whether the $dcp2^{E148Q}$ mutation would alter the aberrant ribosomal profile of *Δdcp1* the *Δdcp1* $dcp2^{E148Q}$ double mutant

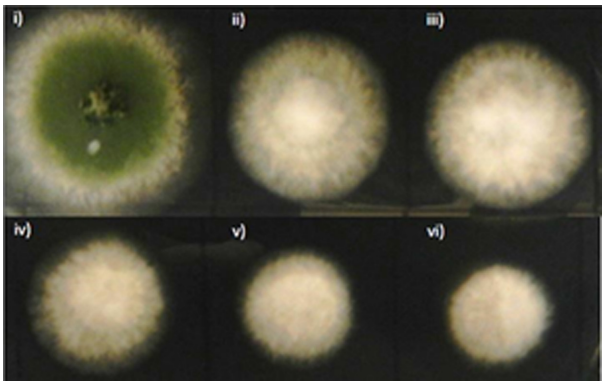

FIGURE 5 Growth morphology of *dcp1* and *dcp2* mutant strains. Phenotypic differences between (i) WT; (ii) Δ*dcp1*; (iii) Δ*dcp2*; (iv) Δ*dcp1* Δ*dcp2*; (v) Δ*dcp1* $dcp2^{E148Q}$; (vi) $dcp2^{E148Q}$ were monitored after growth on solid minimal media at 30°C for 3 days. A similar non-conidiating fluffy phenotype was observed for all mutant strains including the strain with a point mutation targeted to the Nudix domain ($dcp2^{E148Q}$). These data are in concordance with the Nudix domain mutant, $dcp2^{E148Q}$, disrupting the *dcp2* function.

was constructed by crossing the respective single mutants and the resulting strain subjected to the ribosome profiling (Figure 3f). The profile was similar to that of the Δ*dcp1* Δ*dcp2* double mutant (Figure 3e), with the *dcp2*^{E148Q} allele suppressing the Δ*dcp1*-specific profile. Gel electrophoresis of RNA from these ribosomal fractions produced a profile similar to the Δ*dcp2* strain (data not shown). Suppression of the aberrant ribosomal profile of Δ*dcp1* strains in the double mutants, where *dcp2* is either deleted or catalytic activity disrupted, is consistent with the putative degradation product observed in Δ*dcp1* strains resulting, at least in part, from Dcp2-mediated cleavage occurring in the absence of Dcp1.

2.3 | Sequencing of ribosomal repeat in *A. nidulans*

Prior to this work, there was no complete sequence for *A. nidulans* rRNA in any available database. We, therefore, undertook to clone and fully sequence the ribosomal repeat. Divergent primers complementary to the available partial sequence of 18S rRNA (Accession No: U77377) were used to amplify the full rDNA repeat from genomic DNA by PCR. The ~6 kb product, which approximated to the expected size, was cloned into pGEMT-Easy vector and sequenced (Figure S4, NCBI database Accession No. OP613196, OP613218 and OP613197). The sequence of the ribosomal repeat is highly conserved between *Aspergillus* species (Figure S5).

2.4 | Identification of aberrant rRNA fraction expressed by Δ*dcp1* strains

Using the rDNA sequence, we devised probes to investigate whether the putative degradation product observed for Δ*dcp1* strains was derived from the 25S rRNA, using Northern hybridisation analysis. Four different probes were used, one for 18S (the full sequence) and three for 25S; complementary to the 5′ end, the central region and the 3′ end (Figure 6). For all three strains, there were several

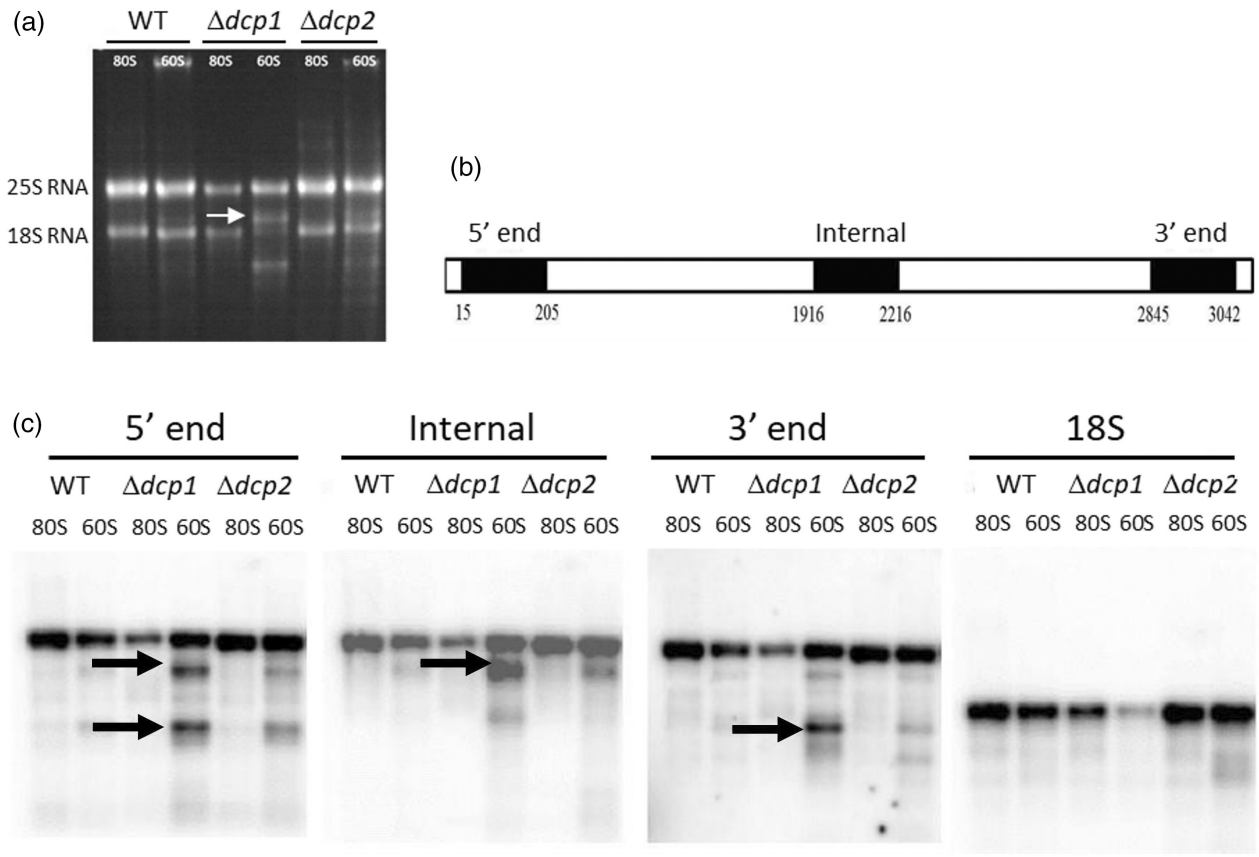

FIGURE 6 Northern blot analysis of rRNA from 80S and 60S ribosomal fractions. (a) Representative images showing gel electrophoresis of the 80S and 60S rRNA fractions from sucrose density centrifugation of cell extracts from wild type (WT), Δ*dcp1* and Δ*dcp2* strains. 2 μg of RNA from each fraction was loaded on a non-denaturing agarose gel. The locations of two major aberrant bands in the Δ*dcp1* 60S fraction are indicated with an arrow. (b) A schematic diagram showing the location of the probes used in Northern blot analysis for the 25S rRNA in *Aspergillus nidulans*. Three different regions of 25S rRNA were selected for probing (5′ end, internal and 3′ end). For 18S, the full DNA sequence was used as a probe. (c) Northern blot analysis using either the 25S 5′ end, internal or 3′ end probes alongside the 18S probe. Major bands which co-localise with those observed in the gel image of the Δ*dcp1* 60S sample are indicated with arrows; the banding pattern changes with the 25S probe used consistent with these being subfractions of the 25S rRNA. In both the gel image and the northern blot, similar but weaker bands are apparent in the Δ*dcp2* and to a lesser extent in the WT sample.

bands that we inferred to be the degradation products of 25S rRNA in the 80S and 60S ribosomes (Figure 6c). However, their relative abundance varied, being dramatically higher (>10 fold) in the *Δdcp1*-derived 60S sample. Based on these results, we propose that cleavage of the 25S rRNA occurs in several positions and that this is not unique to Δ*dcp1* strains but is greatly enhanced in these strains. Interestingly, we observed the dramatic loss of 18S rRNA signal (up to 50% relative to the 80S level) in the Δ*dcp1* 60S fraction compared with WT and Δ*dcp2*. As similar quantities of RNA from each fraction were used, the low signal for 18S rRNA emphasises the dilution effect of the high levels of 25S degradation product in the Δ*dcp1* 60S fraction.

2.5 | Sequencing of 25S degradation products

To further investigate the identity of the 25S "degradation" product derived from the *Δdcp1* strain, we extracted the RNA from a non-denaturing agarose gel and purified it prior to primer ligation and PCR amplification using a small RNA sequencing strategy. Consistent with the northern hybridisation analysis (Figure 6) the sequences obtained were derived from the 5′-end and central region of the 25S rRNA. Of the 15 clones sequenced 14 identical fragments derived from the same 5′-end of 25S rRNA (Figure S4) and only one mapped to the central region. However, the products were 350 and 264 bp in length (Figure S6), which is far shorter than expected based on the migration of the sequence relative to 18S rRNA (>1.5 kb). This inconsistency suggests that the RNA, observed as a single band by non-denaturing gel electrophoresis, is composed of multiple small fragments, which are still bound together in larger structures. This is supported by the analysis of these samples using denaturing polyacrylamide gel electrophoresis which produced a very complex banding pattern (Figure S7). The strong cloning bias towards 5′ end fragments suggests that internal fragments present may be poor cloning substrates. Cleavage of ribosomal RNA has been reported previously (Evguenieva-Hackenberg, 2005; Harhay et al., 2021). These data suggest that disruption of Dcp1 and to a lesser extent Dcp2, promote cleavage and that Dcp2 activity may contribute to some of the cleavage observed.

2.6 | Position of 25S rRNA cleavage sites in the ribosome

To determine the ribosomal location of three cleavage sites identified within the 25S rRNA, we undertook in silico 3D visualisation of the 60S large ribosomal structure (Figure 7). In this analysis, the sequence from the degradation products was aligned with the *S. cerevisiae* 60S ribosomal rRNA (PDB 7b7d). All three mapped cleavage sites show some surface accessibility, consistent with cleavage of the 25S rRNA in the ribosome. Interestingly, the 3′ cleavage sites for both the 5′-end and internal fragments are in proximity within the ribosomal tunnel. The nearby positioning of these two cleavage sites may be significant and consistent with a common cleavage mechanism.

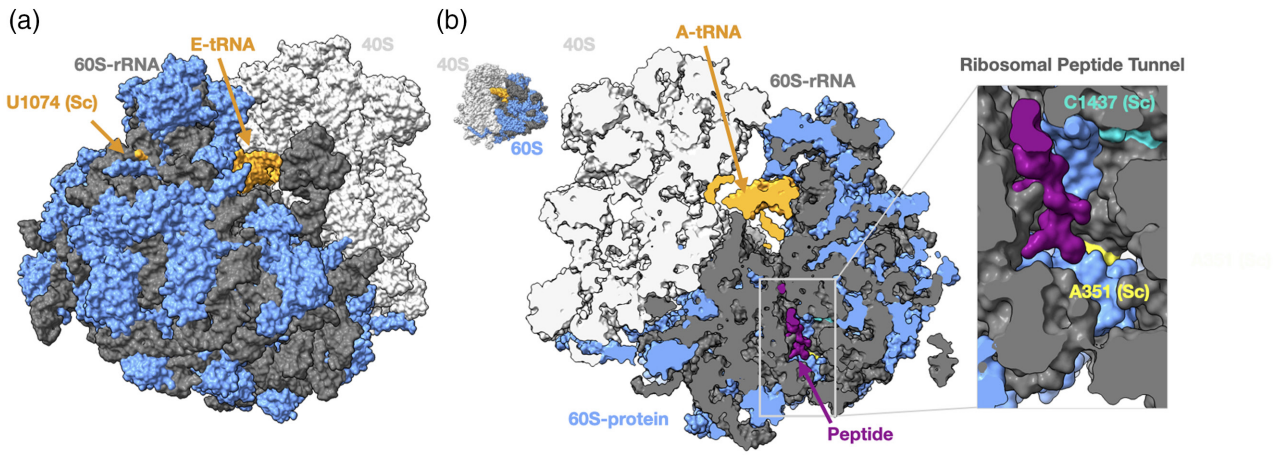

FIGURE 7 Location of 25S rRNA cleavage sites on the ribosome. To predict the location of the cleavage sites in the ribosome structure, the *Aspergillus nidulans* (KY074658.1) and *Saccharomyces cerevisiae* (PDB 7b7d) 25S rRNA sequence were aligned (Clustal Omega) and the alignment used to map the cleavage positions on the structure of the *S. cerevisiae* 80S ribosome. In panels (a) and (b), the 60S subunit is coloured blue (ribosomal proteins) and dark grey (rRNA), and the 40S subunit is light grey. The 3´and 5´residues at the cleavage sites, A351 (3′), U1074 (5′) and C1437 (3′) are coloured yellow, orange, and cyan, respectively. These residues correspond to A336, U1057 and C1420 in *Aspergillus nidulans* (KY074658.1), respectively. In panel (b) the ribosome has been rotated roughly 180° relative to panel (a) and cut through the centre to highlight the location of A351 and C1437 in the ribosomal tunnel. The inset shows a close-up view of the tunnel with a peptide (PDB 7top) showing the path of the nascent chain in the tunnel. For both 25S rRNA fragments identified from the *Δdcp1* strain, the 3′ cleavage sites from the 5′ (A351) and internal (C1437) fragments are in close proximity and within the ribosomal exit tunnel (panel b inset). The close positioning of two fragment 3′ ends might increase the possibility of cleavage in 25S rRNA. The 5′ cleavage site of the internal fragment (A1074) is at the exterior surface of the large subunit.

3 | DISCUSSION

NMD has previously been explored in *A. nidulans* (Morozov et al., 2006, 2012; Mossanen-Parsi et al., 2021), but it had not been determined if either decapping or the principal 5′-3′ exonuclease, Xrn1, are required, as is the situation in *S. cerevisiae* (Muhlrad & Parker, 1994). We tested four mutant strains postulated to disrupt decapping, including the two key decapping factors Dcp1 and Dcp2 and two components associated with the mRNA 3′ end which are involved in initiating the decapping process (Lsm1 and Pat1). We are not aware of the role of Lsm1 in NMD having been previously tested in any organism. These results differentiate *A. nidulans* from *S. cerevisiae*, where decapping is integral to NMD. However, this is more like the situation in mammalian systems where additional mechanisms, including Smg6 that mediated mRNA cleavage, can bypass the requirement for decapping. Furthermore, consistent with decapping not being essential for NMD in *A. nidulans*, the major cytoplasmic 5′-3′ exonuclease, Xrn1, is also not required, implying the 3′-5′ degradation is probably sufficient for NMD in *A. nidulans*. Additionally, no Smg6 orthologue has been reported in any Ascomycete. These observations, therefore, warrant future investigation, to determine if there are additional fungal mechanisms that explain circumvention of the expected NMD dependency on decapping and Xrn1 activity.

While undertaking this aspect of the work, the ribosomal profile obtained by sucrose gradient analysis gave surprising results, with the Δ*dcp1* strain showing an additional major ribosomal band migrating between the 25S and 18S rRNAs. Classically, the individual ribosomal subunits produce two major bands; the 25S rRNA being at the core of the 60S ribosomal subunit, and 18S rRNA of the 40S ribosomal subunit. Northern analysis revealed that the major aberrant product contained the 25S rRNA and was, therefore, derived from the 60S subunit. Our postulation that this represents a degradation product is consistent with it being composed of co-migrating 25S rRNA fragments. The ribosomal RNA has a complex tertiary structure involving multiple interactions between different regions of the rRNA. Thus, if RNA cleavage occurs some of the resulting RNA fragments may still remain associated unless specifically denatured or degraded. This appears to be the situation here. We identified two specific rRNA fragments, both of which are relatively small (~350 nts). As these were obtained from a band migrating between the 25S and 18S rRNAs, they are likely to have remained associated with other co-migrating 25S rRNA fragments. Consistent with this interpretation northern analysis revealed that various regions of the 25S rRNA are present within both this major band and other minor bands observed by non-denaturing gel electrophoresis. We were, therefore, surprised only to clone and sequence two specific fragments. This may represent a shortcoming of our cloning strategy or reflect the type of cleavage and chemical composition of the resulting 5′ and 3′ ends, which may be recalcitrant with respect to conventional ligations strategies.

The northern analysis revealed a range of fragments throughout the gel, derived from both 25S and 18S rRNA, and although the marked profile was specific to the Δ*dcp1* strain, similar less abundant products were apparent in the Δ*dcp2* strain and to a lesser extent in the WT. This is consistent with similar rRNA fragmentation occurring in all three strains suggesting it is a normal process. This is possibly indicative of rRNA degradation and turnover, which is essential to the organism both maintaining and regulating the number of active ribosomes. Ribosomal turnover has been shown to occur by different mechanisms, which involve autophagy (Scott, 1977) and defective ribosomal RNA molecules are specifically targeted for degradation by the process of non-functional ribosomal decay (Cole et al., 2009; Lafontaine, 2010; LaRiviere et al., 2006). There is consistent evidence that subcellular compartmentalisation is integral to these processes, with ribosomal fragmentation and degradation occurring in the vacuole and P-bodies being another structure where non-functional 18S (but not 25S) ribosomal subunits undergo degradation alongside mRNA (Lafontaine, 2010). P-bodies have previously been observed in *A. nidulans* (Morozov, Jones, Spiller, et al., 2010). One intriguing possibility is that the failure to efficiently de-cap mRNA may lead to the accumulation of ribosome or specifically 60S associated mRNAs, which in turn may prompt a degradation process to remove the aberrant complex of ribosome-bound mRNA. Based on our analysis, in the Δ*dcp1* strain (and to a lesser degree in Δ*dcp2*) the levels of active translating ribosomes (polysomes, disomes and monosomes) appear to be very low compared with the ribosomal subunits. This may reflect accumulation of partially degraded, non-functional ribosomal RNA. However, reduced translation may also arise in the Δ*dcp1* strain due to inefficient release of the 60S subunit from the mRNA, which is turn, would inhibit ribosome recycling-mediated translation initiation (Figure 8).

Whether the accumulation of specific rRNA fragments in the Δ*dcp1* strain represents increased fragmentation or a reduced rate of subsequent turnover is a critical question for future investigation. Although outcrosses confirm that the aberrant polyribosomal profile is linked to DCP1 deletion there remains a formal possibility that potential background mutations close to the DCP1 locus or altered expression of a linked gene is responsible for this surprising phenotype. Additionally, deletion of dcp1 is likely to have broad effects of the expression of a wide range of genes as indicated by the gross morphological effects of the mutation. However, the observation that disruption of *dcp2* and specifically the Dcp2 catalytic domain suppresses the aberrant *dcp1* ribosome profile, would suggest that the catalytic domain contributes directly to this process. It seems a possibility that the catalytic domain is, therefore, involved directly in cleaving ribosomal RNA components under these situations, but this is not definitive and in the Δ*dcp1* Δ*dcp2* strain some of this fragmentation did persist, implicating other nuclease activities.

4 | EXPERIMENTAL PROCEDURES

4.1 | *A. nidulans* strains and genetic techniques

A. nidulans markers and the genetic techniques used have been described previously (Clutterbuck, 1974, 1993). Growth media were as described by Cove (1966). Strains deleted for *dcp1*/AN7746

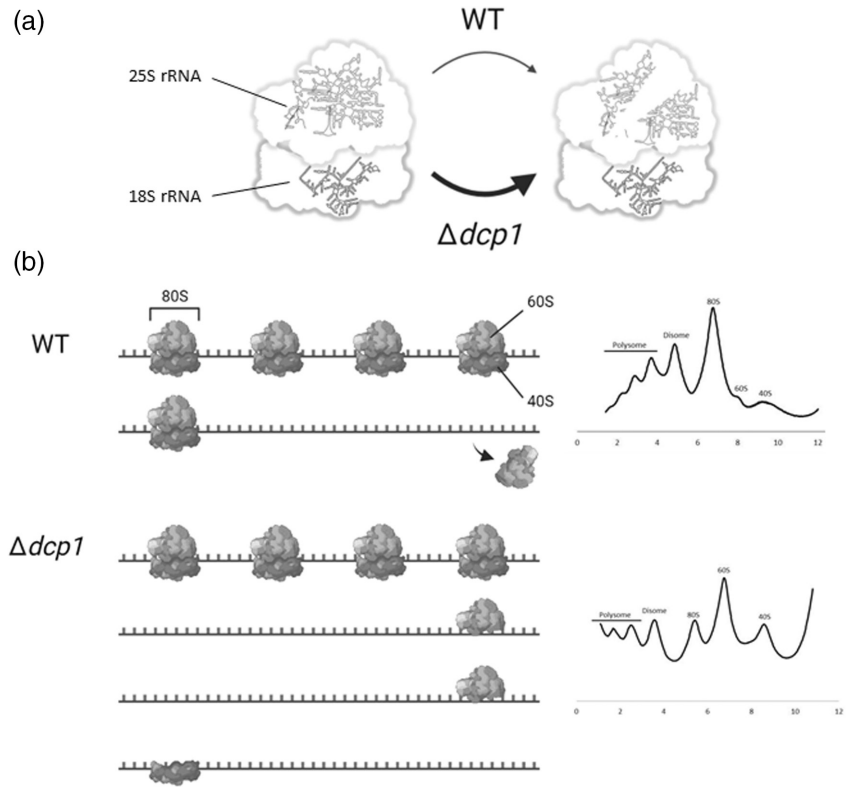

FIGURE 8 A proposed model of the effect of Dcp1 depletion on translation. (a) Depletion for Dcp1 leads to increased degradation of the 25S rRNA in the 60S ribosomal subunit bound to the mRNA. (b) Inactivation of Dcp1 results in an increased abundance of mRNAs associated with the 60S ribosomal subunit, possibly related to attenuated translation termination. This would be consistent with the relatively low levels of actively translating ribosomes associated with a decrease in 80S formation and a simultaneous increase in 40S ribosomal subunit levels, possibly due to an insufficient supply of functional 60S.

and *dpc2*/AN10010, *dhh1*/AN10417, *lsm1*/AN6199, *pat1*/AN2751, and *xrn1*/AN11052 were described previously (Mossanen-Parsi et al., 2021). The strain bearing the *dcp2*^{E148Q} allele was constructed by gene replacement using a linear copy of the full gene, engineered and amplified by PCR using Phusion High-Fidelity DNA Polymerases (Thermo Scientific). The recombinant PCR construct was transformed into a strain with the genotype; Δ*dcp2*::Af-pyrG (*pyrG89) pyroA4*; *nkuA*::*argB*. Knock-in transformants were selected on the basis 5-fluoroorotic acid resistance, resulting from loss of *Af-pyrG* (Szewczyk et al., 2006). Fidelity of the resulting strain was confirmed by PCR, Southern hybridisation and sequencing. Additionally, the mutant strain was outcrossed to confirm the mendelian segregation of the phenotype. Strains bearing double or treble mutants were constructed by standard genetic crosses and confirmed by PCR. The strains and oligonucleotide primers used in this study are listed in Tables S1 and S2, respectively.

4.2 | Transcript and ribosome analysis

Growth of mycelia, RNA preparation and quantitative northern analysis were described previously (Caddick et al., 2006; Morozov et al., 2000). Briefly, overnight cultures were incubated at 30°C for 14–16 h with shaking. Fully supplemented minimal media was used with uric acid as the sole nitrogen source. Quantitative real-time polymerase PCR was used to monitor transcript levels. For each sample, 2 μg of total RNA was reverse transcribed with random hexamers using the Tetro reverse transcriptase (Bioline). Three transcripts were investigated in this study; *uaZ*, *hxA* and 18S rRNA as the internal control. The sequences of the PCR primers are given in Table S2. PCR reactions of 20 μL were set up with 10 μL 2X SensiFAST SYBR Hi-ROX Kit (Bioline). PCRs were conducted using the StepOnePlus™ Real-Time PCR System (Applied Biosystems) with the following settings: 2 min at 95°C, 40 amplification cycles (every 5 s at 95°C, 10 s annealing at 57°C, and 5 s at 72°C with endpoint fluorescence detection). Gene expression analysis was carried out using comparative Ct method (Livak & Schmittgen, 2001). Polysome fractionation was achieved using sucrose gradients as previously described (Morozov, Jones, Razak, et al., 2010). For Northern hybridisation, two types of agarose gels were used, which are the non-denaturing and denaturing gels. For non-denaturing gel, agarose gel electrophoresis used 1% (w/v) agarose (Bioline) in 1 × TAE (0.4 M Tris-acetate, 1 mM EDTA). For denaturing agarose gel electrophoresis used 1% (w/v) agarose (Bioline) in 1 × MOPS buffer and 2% (w/v) formaldehyde. RNA samples were prepared by adding 10 μL 2X sample buffer (50 μL formamide, 18 μL 37% formaldehyde, 10 μL 10X MOPS buffer and 3 μL 10X Dye Solution [50% glycerol, 0.3% Bromophenol Blue]). Samples were denatured at 65°C for 10 min and transferred to ice prior to loading. The gel was submerged in 1X MOPS and the samples were run for 3 h at 100 V. After electrophoresis, the RNA was transferred to Zeta-Probe GT (BioRad) blotting membrane. The membrane was hybridised to radiolabelled (α^{32}P – dCTP) DNA probes at 65°C followed the recommended protocols for Zeta-Probe membrane. Imaging was conducted using a Molecular Dynamics STORM™ scanner and quantification was done using ImageQuant TL Software (GE Healthcare Life Sciences).

4.3 | Ribosomal repeat, cloning and sequencing

The partial sequence of 18S rRNA (Accession No: U77377) was used as a reference to design the primers to amplify the full ribosomal repeat—18S-Fwd-out: 5′ ACACCGCCTGTCGCTACTAC, 18S-Rev-out: 5′ AATGAGCCATTCGCAGTTTC. PCR was conducted using KOD Hot-Start DNA Polymerase (Sigma-Aldrich). The amplified PCR product with the expected size of ~6 kb was purified and cloned into pGEMT-Easy vector and Sanger sequenced. For the Northern hybridisation analysis, the PCR primers for probe construction are listed in Table S2.

4.4 | Small RNA cloning procedure and sequencing

Non-denaturing agarose gel electrophoresis was used to isolate the major band of "degradation" products derived from the Δ*dcp1* strain. The RNA was purified using the QIAquick Gel Extraction Kit (Qiagen). The purified RNA was then ligated with RNA adapters. This and subsequent cDNA synthesis and PCR amplification followed the NEB Next® Multiplex Small RNA Library Prep protocol. The PCR products were cloned into pMiniT and subjected to sanger sequencing.

AUTHOR CONTRIBUTIONS

Izwan Bharudin: Methodology; Funding acquisition; Visualization; Data curation; Formal analysis; Investigation; Writing—review & editing. Mark X. Caddick: Conceptualization; Investigation; Funding acquisition; Writing—original draft; Methodology; Validation; Visualization; Writing—review & editing; Formal analysis; Data curation; Supervision. Sean R. Connell: Investigation; Writing—original draft; Methodology; Visualization; Writing—review & editing; Formal analysis. Matthew T. F. Lamaudière: Investigation; Visualization; Writing—review & editing; Data curation; Methodology. Igor Y. Morozov: Conceptualization; Investigation; Writing—original draft; Methodology; Validation; Writing—review & editing; Formal analysis; Project administration; Supervision.

ACKNOWLEDGMENTS

This work was supported by grants from the BBSRC (BB/H020365) to MXC to support IYM. the Ministerio de Economía Y Competitividad Grant (MINECO; PID2021-122705OB-I00 and CTQ201782222-R) to Paola Fucini and S.R.C. Gene analysis and orthologue identification used the FungiDB database.

DATA AVAILABILITY STATEMENT

The data that support the findings of this study are available from the corresponding author upon reasonable request.

ETHICS STATEMENT

No human or animal models/samples have been used in this work.

ORCID

Igor Y. Morozov https://orcid.org/0000-0003-0927-0309

REFERENCES

Amberg, D.C., Goldstein, A.L. & Cole, C.N. (1992) Isolation and characterization of RAT1: an essential gene of *Saccharomyces cerevisiae* required for the efficient nucleocytoplasmic trafficking of mRNA. *Genes & Development*, *6*, 1173–1189.

Caddick, M.X., Jones, M.G., van Tonder, J.M., Le Cordier, H., Narendja, F., Strauss, J. et al. (2006) Opposing signals differentially regulate transcript stability in *Aspergillus nidulans*. *Molecular Microbiology*, *62*, 509–519.

Cao, D. & Parker, R. (2003) Computational modeling and experimental analysis of nonsense-mediated decay in yeast. *Cell*, *113*, 533–545.

Celik, A., He, F. & Jacobson, A. (2017) NMD monitors translational fidelity 24/7. *Current Genetics*, *63*, 1007–1010.

Chang, C.-T., Bercovich, N., Loh, B., Jonas, S. & Izaurralde, E. (2014) The activation of the decapping enzyme DCP2 by DCP1 occurs on the EDC4 scaffold and involves a conserved loop in DCP1. *Nucleic Acids Research*, *42*, 5217–5233.

Clutterbuck, A.J. (1974) *Aspergillus nidulans*. New York: Plenum Press.

Clutterbuck, A.J. (1993) *Aspergillus nidulans*. Cold Spring Harbor, NY: Cold Spring Harbor Laboratory Press.

Cole, S.E., LaRiviere, F.J., Merrikh, C.N. & Moore, M.J. (2009) A convergence of rRNA and mRNA quality control pathways revealed by mechanistic analysis of nonfunctional rRNA decay. *Molecular Cell*, *34*, 440–450.

Coller, J. & Parker, R. (2004) Eukaryotic mRNA decapping. *Annual Review of Biochemistry*, *73*, 861–890.

Cove, D.J. (1966) Induction and repression of nitrate reductase in fungus *Aspergillus nidulans*. *Biochimica et Biophysica Acta*, *113*, 51–56.

Evguenieva-Hackenberg, E. (2005) Bacterial ribosomal RNA in pieces. *Molecular Microbiology*, *57*, 318–325.

Harhay, G.P., Harhay, D.M., Brader, K.D. & Smith, T.P.L. (2021) A conserved *Histophilus somni* 23S intervening sequence yields functional, fragmented 23S rRNA. *Microbiology Spectrum*, *9*, e01431-01421.

Hu, W., Sweet, T.J., Chamnongpol, S., Baker, K.E. & Coller, J. (2009) Co-translational mRNA decay in *Saccharomyces cerevisiae*. *Nature*, *461*, 225–229.

Huntzinger, E., Kashima, I., Fauser, M., Saulière, J. & Izaurralde, E. (2008) SMG6 is the catalytic endonuclease that cleaves mRNAs containing nonsense codons in metazoan. *RNA*, *14*, 2609–2617.

Kervestin, S. & Jacobson, A. (2012) NMD: a multifaceted response to premature translational termination. *Nature Reviews Molecular Cell Biology*, *13*, 700–712.

Lafontaine, D.L.J. (2010) A "garbage can" for ribosomes: how eukaryotes degrade their ribosomes. *Trends in Biochemical Sciences*, *35*, 267–277.

LaRiviere, F.J., Cole, S.E., Ferullo, D.J. & Moore, M.J. (2006) A late-acting quality control process for mature eukaryotic rRNAs. *Molecular Cell*, *24*, 619–626.

Livak, K.J. & Schmittgen, T.D. (2001) Analysis of relative gene expression data using real-time quantitative PCR and the 2−ΔΔCT method. *Methods*, *25*, 402–408.

Morozov, I.Y., Jones, M.G., Gould, P.D., Crome, V., Wilson, J.B., Hall, A.J.W. et al. (2012) mRNA 3′ tagging is induced by nonsense-mediated decay and promotes ribosome dissociation. *Molecular and Cellular Biology*, *32*, 2585–2595.

Morozov, I.Y., Jones, M.G., Razak, A.A., Rigden, D.J. & Caddick, M.X. (2010) CUCU modification of mRNA promotes Decapping and transcript degradation in *Aspergillus nidulans*. *Molecular and Cellular Biology*, *30*, 460–469.

Morozov, I.Y., Jones, M.G., Spiller, D.G., Rigden, D.J., Dattenböck, C., Novotny, R. et al. (2010) Distinct roles for Caf1, Ccr4, Edc3 and CutA in the

co-ordination of transcript deadenylation, decapping and P-body formation in *Aspergillus nidulans*. *Molecular Microbiology*, *76*, 503–516.
Morozov, I.Y., Martinez, M.G., Jones, M.G. & Caddick, M.X. (2000) A defined sequence within the 3′ UTR of the areA transcript is sufficient to mediate nitrogen metabolite signalling via accelerated deadenylation. *Molecular Microbiology*, *37*, 1248–1257.
Morozov, I.Y., Negrete-Urtasun, S., Tilburn, J., Jansen, C.A., Caddick, M.X. & Arst, H.N. (2006) Nonsense-mediated mRNA decay mutation in *Aspergillus nidulans*. *Eukaryotic Cell*, *5*, 1838–1846.
Mossanen-Parsi, A., Parisi, D., Browne-Marke, N., Bharudin, I., Connell, S.R., Mayans, O. et al. (2021) Histone mRNA is subject to 3′ uridylation and re-adenylation in *Aspergillus nidulans*. *Molecular Microbiology*, *115*, 238–254.
Muhlrad, D. & Parker, R. (1994) Premature translational termination triggers mRNA decapping. *Nature*, *370*, 578–581.
Muhlrad, D. & Parker, R. (1999) Recognition of yeast mRNAs as "nonsense containing" leads to both inhibition of mRNA translation and mRNA degradation: implications for the control of mRNA Decapping. *Molecular Biology of the Cell*, *10*, 3971–3978.
Nagarajan, V.K., Jones, C.I., Newbury, S.F. & Green, P.J. (2013) XRN 5′→3′ exoribonucleases: structure, mechanisms and functions. *Biochimica et Biophysica Acta (BBA) - Gene Regulatory Mechanisms*, *1829*, 590–603.
Nissan, T., Rajyaguru, P., She, M., Song, H. & Parker, R. (2010) Decapping activators in *Saccharomyces cerevisiae* act by multiple mechanisms. *Molecular Cell*, *39*, 773–783.
Rissland, O.S. & Norbury, C.J. (2009) Decapping is preceded by 3′ uridylation in a novel pathway of bulk mRNA turnover. *Nature Structural & Molecular Biology*, *16*, 616–623.
Scott, J.F. (1977) Turnover of ribosomal RNA in cells in culture. *Experimental Cell Research*, *108*, 207–219.
Song, M.-G., Bail, S. & Kiledjian, M. (2013) Multiple Nudix family proteins possess mRNA decapping activity. *RNA*, *19*, 390–399.
Szewczyk, E., Nayak, T., Oakley, C.E., Edgerton, H., Xiong, Y., Taheri-Talesh, N. et al. (2006) Fusion PCR and gene targeting in *Aspergillus nidulans*. *Nature Protocols*, *1*, 3111–3120.
Valkov, E., Muthukumar, S., Chang, C.-T., Jonas, S., Weichenrieder, O. & Izaurralde, E. (2016) Structure of the Dcp2–Dcp1 mRNA-decapping complex in the activated conformation. *Nature Structural & Molecular Biology*, *23*, 574–579.
Vidya, E. & Duchaine, T.F. (2022) Eukaryotic mRNA Decapping activation. *Frontiers in Genetics*, *13*, 832547.
Xing, W., Muhlrad, D., Parker, R. & Rosen, M.K. (2020) A quantitative inventory of yeast P body proteins reveals principles of composition and specificity. *eLife*, *9*, e56525.

SUPPORTING INFORMATION

Additional supporting information can be found online in the Supporting Information section at the end of this article.

How to cite this article: Bharudin, I., Caddick, M. X., Connell, S. R., Lamaudière, M. T. F. & Morozov, I. Y. (2023). Disruption of Dcp1 leads to a Dcp2-dependent aberrant ribosome profiles in *Aspergillus nidulans*. *Molecular Microbiology*, *00*, 1–10. https://doi.org/10.1111/mmi.15059